Proceedings of the
44th IEEE Conference on Decision and Control, and
the European Control Conference 2005
Seville, Spain, December 12-15, 2005

Optimal refractive index profile design for a pair of optical fibre-based devices.*

Peter M. Dower† p.dower@ee.unimelb.edu.au
Peter M. Farrell‡ p.farrell@ee.unimelb.edu.au
†,‡ Department of Electrical and Electronic Engineering
The University of Melbourne, Australia

***Abstract*— This paper presents an application of nonlinear optimization in the design of two particular optical fibre-based devices, namely an evanescent field sensor and a communications fibre. This work formalizes and improves upon ad-hoc methods employed in the optics literature and results in some quite novel device designs of current interest to the photonics community. The tools applied include dynamic programming and an implicit Markov chain approximation method for numerically solving the attendant dynamic programming equation.**

***Keywords*— Optimization, refractive index design, dynamic programming, optical fibre sensor design, refractive index profile.**

I. Introduction

Optical fibre-based devices are finding increasing application in a wide range of fields, from biomedicine through to telecommunications. Fundamental to the operation of such devices is the *refractive index profile*, which describes a spatial property of the silica substrate that determines if and how electromagnetic radiation is guided through the device. The selection of the refractive index profile, illustrated in Figure 1, is thus vital in the design of many optical devices such as sensors, couplers and communications fibres. This paper considers the problem of optimal refractive index selection for such optical devices.

II. An electric field model for optical fibres

A given optical fibre with known profile n_f immersed in an environment of known refractive index n_e typically supports a number of *modes* of electric field propagation, each defined by a *modal parameter pair* (l, β), where $l \in \mathbf{Z}$ is the *separation constant* and $\beta \in \mathbf{R}$ is the *propagation constant*. The electric field, a vector denoted $\mathbf{E}_{l,\beta,n}(r, \phi, z)$, for the given triple (l, β, n) is then

$$\mathbf{E}_{l,\beta,n}(r, \phi, z) \;=\; \mathbf{\Psi}_{l,\beta,n}(r, \phi) e^{j\beta z}, \qquad (1)$$

where (r, ϕ, z) is the radially normalized cylindrical coordinate position (inside or outside the fibre), $\mathbf{\Psi}_{l,\beta,n} : \mathbf{R}^2 \to \mathbf{R}^3$ is a vector valued function of this cylindrical coordinate position, $n := n_f \cup n_e$ is the concatenated fibre / environment profile, and $j = \sqrt{-1}$. Where the resulting optical fibre model is linear, superposition can be applied to yield the total electric field in the presence of all supported modes.

*This research was partially supported by the Australian Research Council.

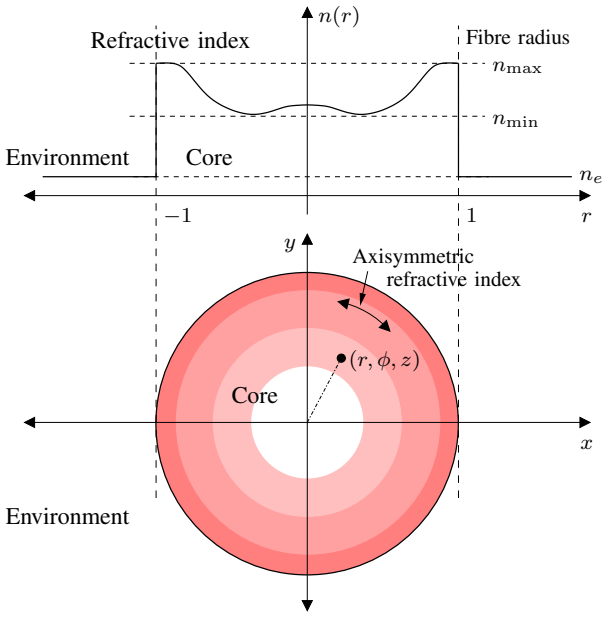

Fig. 1. An optical fibre cross-section.

As a matter of interpretation, it is important to note that the electric field (1) of a particular propagating mode also contains an implicit time dependence $e^{-j\omega t}$, so that each mode must have a *phase velocity* of $v = \frac{\omega}{\beta}$. This phase velocity can be used to quantify the rate at which signal features propagate along an optical fibre, and is clearly dependent on the particular mode. Although different phase velocities give rise to chromatic dispersion in optical fibres, this issue is not considered here. Nonlinear refraction due to high intensity electric fields is also ignored. Rather, attention is restricted to a single mode of low intensity electric field propagation, as defined by a single modal parameter pair (l, β), for the given profile. Further to this, we utilizes the following physically motivated properties of optical fibres:

(I) The optical fibre is *axisymmetric* and *translationally invariant*, with a refractive index profile $n \in \mathcal{N}_\infty(0, 1]$.

(E) The refractive index $n_e \in \mathcal{N}_0(1, \infty)$ of the environment surrounding the fibre sensor is constant. That is, $n_e(r) \equiv n_e \in \mathbf{R}_{\geq 0}$ for all $r \in (1, \infty)$.

(G) The refractive index profile of the optical fibre satisfies the following:

1) (Internal reflection) The minimum refractive index $n_{\min}$ utilized in the device is greater than that of

the surrounding cladding or environment. That is, $n_e \leq n_{\text{cl}} < n_{\min}$.

2) (Phase velocity) The phase velocity of the propagating mode (1) defined by the modal parameter pair (l, β) is bounded by the minimum and maximum speed of light attained across the optical fibre and the environment. Consequently, the propagation constant must satisfy

$$n_e k \ < \ \beta \ < \ n_{\max} k, \tag{2}$$

where $k = \frac{2\pi}{\lambda}$ is the *wave number*, and λ is the *wavelength* of the propagating radiation.

(P) The *evanescent field* power is finite.

For the purpose of presenting a simple special case, the following additional physical property is sometimes considered:

(W) The *weak guidance* approximation [8] holds.

Here, $\mathcal{N}_0(r_0, r_1]$ and $\mathcal{N}_\infty(r_0, r_1]$ are defined respectively as the spaces of piecewise constant and piecewise continuous functions on the normalized radial interval $(r_0, r_1]$. (Note that notions of evanescent field and weak guidance will be defined later.)

In asserting the invariance property **(I)** and ignoring the effects of polarization as per property **(W)**, only the *transverse* electric field need be considered [8]. That is, the electric field coefficient $\mathbf{\Psi}_{l,\beta,n}$ has a component in the radial cylindrical coordinate direction only (there are no components in the longitudinal z or angular ϕ directions). However, this radial component remains a function of both the radial and angular cylindrical coordinates (r, ϕ). Where these radial and angular dependencies are separable (as turns out to be the case in the presence of properties **(I)** and **(W)**), $\mathbf{\Psi}_{l,\beta,n}$ can be expressed as

$$\mathbf{\Psi}_{l,\beta,n}(r,\phi) \ = \ \psi_{l,\beta,n}(r,\phi)\hat{\mathbf{r}} \ = \ F_{l,\beta,n}(r)\Phi_l(\phi)\hat{\mathbf{r}}, \tag{3}$$

where $\psi_{l,\beta,n} : \mathbf{R} \times \mathbf{R} \to \mathbf{R}$ is a scalar valued function of the cylindrical coordinate pair (r, ϕ), $F_{l,\beta,n} : \mathbf{R} \to \mathbf{R}$ is a scalar valued function of the radial coordinate, $\Phi_l : \mathbf{R} \to \mathbf{R}$ is a scalar valued function of the angular coordinate, and $\hat{\mathbf{r}}$ is the unit radial cylindrical coordinate vector.

Under the listed properties presented, the physical setup of interest can thus be modelled by (1), (3), and the scalar wave equation (SWE)

$$\begin{aligned}\left\{\nabla_t^2 + k^2 n(r)^2 - \beta^2\right\}\psi_{l,\beta,n}(r,\phi) + \\ \frac{\partial}{\partial r}\left[\psi_{l,\beta,n}(r,\phi)\tfrac{d\ \ln[n(r)^2]}{dr}\right] = 0,\end{aligned} \tag{4}$$

where ∇_t is the transverse Laplacian operator, and $n(\cdot)$ is the refractive index profile. Further simplification via (3) yields the separated scalar wave equation (SSWE)

$$\begin{aligned}\left\{\tfrac{d^2}{dr^2} + \left(\tfrac{1}{r} + \tfrac{d\ln[n(r)^2]}{dr}\right)\tfrac{d}{dr} + k^2R^2\left[n(r)^2 - n_{\text{eff}}^2\right]\right. \\ \left. -\tfrac{l^2}{r^2} + \tfrac{d^2\ln[n(r)^2]}{dr^2}\right\} F_{l,\beta,n}(r) \ = \ 0\end{aligned} \tag{5}$$

It is important to note that in the case of piecewise constant refractive index profiles (i.e. $n \in \mathcal{N}_0(0,1]$), SSWE (5) reduces to a *linear second order* ODE almost everywhere,

$$\left\{\tfrac{d^2}{dr^2} + \tfrac{1}{r}\tfrac{d}{dr} + k^2R^2\left[n(r)^2 - n_{\text{eff}}^2\right] - \tfrac{l^2}{r^2}\right\} F_{l,\beta,n}(r) \ = \ 0. \tag{6}$$

Solution pieces of (6) connected via continuity thus form solutions of (5). Boundary conditions for both (5) and (6) impose differentiability of the field along the fibre axis, and finiteness of the evanescent field power (property **(P)**). These conditions are listed respectively below:

$$\left.\begin{array}{l} lF_{l,\beta,n}(0) = 0 \\ \frac{dF_{l,\beta,n}}{dr}(0) = 0 \end{array}\right\} \quad \text{and} \quad \frac{dF_{l,\beta,n}}{dr}(1) = \gamma_{l,\beta,n_e}F_{l,\beta,n}(1). \tag{7}$$

Here, γ_{l,β,n_e} is a constant determined by the modal parameter pair (l, β) and the refractive index n_e of the environment.

For the purpose of later analysis, a state vector suitable for (6) is

$$x := \begin{bmatrix} x_1 \\ x_2 \\ x_3 \\ x_4 \end{bmatrix} \equiv \begin{bmatrix} F_{l,\beta,n} \\ \frac{dF_{l,\beta,n}}{dr} \\ \eta \\ \tau \end{bmatrix}, \tag{8}$$

where the refractive index dependency η is augmented to allow consideration of refractive index rate constraints, and τ is the spatial coordinate satisfying $\dot{\tau} = 1$. In that case, the corresponding nonlinear state space representation is then

$$\dot{x}(r) = f(x(r), u(r)), \tag{9}$$

where

$$f(x,u) := \left[\begin{array}{cc|c} 0 & 1 & \mathbf{0} \\ \frac{l^2}{x_4^2} - x_3 & -\frac{1}{x_4} & \\ \hline \multicolumn{2}{c|}{\mathbf{0}} & \mathbf{0} \end{array}\right] x + \begin{bmatrix} \mathbf{0} \\ \mathbf{e}_1 \end{bmatrix} u + \begin{bmatrix} \mathbf{0} \\ \mathbf{e}_2 \end{bmatrix}$$

where $\mathbf{e}_1 := [1 \ 0]'$, $\mathbf{e}_2 := [0 \ 1]'$. The refractive index $n \in \mathcal{N}(0,1]$ can be recovered from the state trajectory $x : (0,1] \to \mathbf{R}^4$ via

$$n(r) := \sqrt{n_{\text{eff}}^2 + \frac{x_3(r)}{k^2R^2}}. \tag{10}$$

Here, n_{eff} is the *effective refractive index* of the optical fibre, as seen by the mode $\mathbf{E}_{l,\beta,n}$ with modal parameter pair (l, β). The definition of n_{eff} is motivated by constraint (2), and is given by

$$n_{\text{eff}} \ := \ \frac{\beta}{k}. \tag{11}$$

It is important to note that in practice, the refractive index n and refractive index rate $\frac{dn}{dr}$ are constrained by the manufacturing process. These constraints can be measured or computed, and correspond to a state constraint on x_3 and an input constraint on u, denoted respectively by $x_3(r) \in \mathbf{X}_3 := [\eta_{\min}, \eta_{\max}]$ and $u(r) \in \mathbf{U} := [u_{\min}, u_{\max}]$ for all $r \in (0,1]$. Similarly, state constraints on the field x_1 and field derivative x_2 may also be required to avoid severe nonlinear optical effects due to the dependence of the refractive index on field intensity and wavelength. Formally, all such state constraints can be denoted by

$$x(r) \in \mathbf{X} := \cup_i \mathbf{X}_i \subset \mathbf{R}^4, \quad r \in (r_\circ, 1], \tag{12}$$

where $r_\circ > 0$ is selected arbitrarily small (but non-zero to avoid degeneracy in (9)), and the end points of the intervals $\mathbf{X}_i \subset \mathbf{R}$ are selected according to various design requirements. In addition, boundary conditions (7) also give rise to other state constraints. In particular,

$$\left\{ \begin{array}{rcl} l x_1(r_\circ) & = & 0 \\ x_2(r_\circ) & = & 0 \\ x_4(r_\circ) & = & r_\circ \end{array} \right. \tag{13}$$

and

$$\left\{ \begin{array}{rcl} x_2(1) & = & \gamma_{l,\beta,n_e} x_1(1) \\ x_3(1) & = & k^2 R^2 \left(n_{\rm cl}^2 - n_{\rm eff}^2 \right) \\ x_4(1) & = & 1 \end{array} \right. \tag{14}$$

(Note that the last constraint in (14) is automatic from (13) and (9).) At an infinite distance from the fibre, the field and field derivative are necessary zero by property **(P)**. Hence,

$$\left\{ \begin{array}{rcl} x_1(\infty) & = & 0 \\ x_2(\infty) & = & 0 \end{array} \right. \tag{15}$$

Where the cladding and environment refractive indices $n_{\rm cl}$ and n_e are different, a discontinuity in x_3 occurs at the outer cladding radius $R_{\rm cl} > 1$, as $x_3(1) = n_{\rm cl}$ and $x_3(\infty) = n_e$. However, as the refractive index profile formed by $n_{\rm cl}$ and n_e is fixed and piecewise constant, this is not a problem as the field can be determined explicitly (and exactly) from (6) in modified Bessel function form [8] for all $r > 1$.

III. An optimal design approach

A crucial defining aspect of an optimal device design can now be described. Through the application of the aforementioned model, the electric field associated with a electromagnetic wave coaxially propagating through the fibre can now be understood and determined both *inside* and *outside* the optical fibre. The component of the field propagating outside, called the *evanescent field*, is precisely that which interacts with the surrounding environment. Maximizing the relative power of the evanescent field (compared with the total field power) is thus of immediate importance in designing such evanescent field optical fibre sensors. Similarly, minimizing this relative power is of interest in communications fibre design. Thus the performance measure used in both optimal device designs is relative field power, as defined by

$$\overline{\mathcal{P}}(\mathbf{E}_{l,\beta,n}) \;:=\; \frac{\hat{\mathcal{P}}(1,\infty;\mathbf{E}_{l,\beta,n})}{\hat{\mathcal{P}}(0,\infty;\mathbf{E}_{l,\beta,n})} \;=\; \frac{\mathcal{P}(1,\infty;F_{l,\beta,n})}{\mathcal{P}(0,\infty;F_{l,\beta,n})} \tag{16}$$

where

$$\begin{array}{rcl} \hat{\mathcal{P}}(r_1,r_2;\mathbf{E}_{l,\beta,n}) & := & \displaystyle\int_{r_1}^{r_2} s F_{l,\beta,n}(r)^2 \, dr \int_0^{2\pi} \Phi_l(\phi)^2 \, d\phi \\ & = & \mathcal{P}(r_1,r_2;F_{l,\beta,n}) \cdot \mathcal{Q}(\Phi_l). \end{array}$$

The field dynamics underlying (16) are described by the SSWE (6), whilst the optimizing input that constitutes the "design" is the refractive index profile $n \in \mathcal{N}(0,1]$ of the fibre itself. (Note that in lieu of model (9), the refractive index *rate* would actually be designed first, with n recovered using (10).) One technique for expressing this optimization problem in a more conventional form was presented in [2] and further developed in [3]. The remainder of this paper will focus on the application of this and other techniques to two particular device design problems.

IV. Sensor design

A. Theory

In designing evanescent field sensor, the emphasis is on maximizing the relative evanescent field power (16) subject to the dynamics (9), constraints (12), and boundary conditions (13), (14) and (15). Specifically, the maximizing refractive index profile $n^* \in \mathcal{N}(0,1]$ (see [2], [3]) or rate profile $u^* \in \mathcal{U}(0,1]$ is sought, where

$$u^* := \operatorname*{argmax}_{u \in \mathcal{U}(0,1]} \left\{ \overline{\mathcal{P}}(\mathbf{E}_{l,\beta,n}) \;\middle|\; \begin{array}{c} \text{(9), (12), (13)} \\ \text{(14), (15) hold} \end{array} \right\}, \tag{17}$$

and $\mathcal{U}(0,1]$ is the space of bounded functions $u : (0,1] \to \mathbf{U}$. A dynamic programming approach to solving a simpler problem was presented in [2], [3]. This extends to this case, requiring computation of two associated value functions:

$$\Pi^C_{l,\beta}(x) \;=\; \inf_{u \in \mathcal{U}(0,1]} \left\{ \mathcal{P}(0,1;F_{l,\beta,n}) \;\middle|\; \begin{array}{l} \text{(8), (9), (12)} \\ \text{and (13) hold} \\ \text{with } x(1) = x \end{array} \right\} \tag{18}$$

$$\Pi^E_{l,\beta}(x) \;=\; \mathcal{P}(1,\infty;F_{l,\beta,n_e}) \;\middle|\; \begin{array}{l} \text{(8), (9), (12)} \\ \text{and (15) hold} \end{array} \tag{19}$$

As indicated in [2], [3], $\Pi^E_{l,\beta}$ can be computed numerically by direct integration. However, computation of $\Pi^C_{l,\beta}$ is achieved via utilizing an approximating Markov chain method [7], the particular adaptation of which is documented in the Appendix. The dynamic programming equation (DPE) considered on $\mathbf{X}$ is

$$0 = x_1^2 x_4 - \sup_{u \in \mathbf{U}} \left\{ \nabla_x \Pi^C_{l,\beta}(x) \cdot f(x,u) \right\}, \tag{20}$$

where x and f are as per (8) and (9) respectively, and $\Pi^C_{l,\beta}$ is initialized as per (21). The boundary conditions associated with (20) are summarized by

$$\Pi^C_{l,\beta}(x) = \left\{ \begin{array}{ll} 0 & \text{wherever (13) holds,} \\ & \text{and } x \in \partial\mathbf{X}, \\ \infty & \text{elsewhere in } \partial\mathbf{X}. \end{array} \right. \tag{21}$$

(Here, $\partial\mathbf{X}$ denotes the boundary of the set $\mathbf{X}$.)

With value functions (18) and (19) computed, the recipe presented in [3] yields the optimal refractive index profile. In particular, the optimal refractive index or rate is the optimal input $u^* \in \mathcal{U}(0,1]$ determined by integrating the "closed loop system" comprised of (9) and the state feedback characterization of the optimal decision policy determined by (20), initialized with the *minimizing interface state* $x_{\rm int} \in \mathbf{R}^4$ at the fibre / cladding (or environment) boundary, towards the axis of the fibre. The process of determining this crucial minimizing interface state is modified from that in [3], and is defined (and computed) as follows:

$$x_{\rm int} = \operatorname*{argmin}_{x \in \mathbf{R}^4} \left\{ \Pi^C_{l,\beta}(x) \;\middle|\; \begin{array}{c} \Pi^C_{l,\beta}(x) + \Pi^E_{l,\beta}(x) = 1 \\ \text{and (14) holds} \end{array} \right\} \tag{22}$$

In those cases where the cladding refractive index is also free, the boundary condition $x_3(1) = n_{\rm cl}$ should be relaxed in (14), requiring a more extensive search in computing (22).

Finally, before presenting the particular design problems of interest, it is interesting to note that the optimizing input $u^* \in \mathcal{U}(0,1]$ defined as indicated above has a tendency to be "bang-bang" in nature, at least away from the boundary conditions. This is particularly important where refractive index rate constraints are *not* considered, as this necessarily gives rise to refractive index profiles that oscillate between the refractive index limits $n_{\min}$ and $n_{\max}$ allowable. Significantly, these types of profiles correspond well to recently discovered *holey fibre structures* [1], [6] that are of increasing interest in the optical sensing community.

B. Case I: Refractive index design without rate constraints

A fibre sensor with the following physical parameters is to be designed:

$$\begin{array}{rclrcl} n_{\min} & = & 1.456 & R & = & 5\,\mu m \\ n_{\max} & = & 1.600 & \lambda & = & 850\,nm \\ n_e & = & 1.333 & l & = & 0 \\ n_{\rm eff} & = & 1.476 & \beta & = & 1.091 \times 10^7\, m^{-1} \\ n_{\rm cl} & = & n_{\min} & \gamma_{l,\beta,n_e} & = & -23.90 \end{array}$$

Without refractive index rate constraints, the solution of this design problem is as per [3], yielding the value function $\Pi^C_{l,\beta}$ as per Figure 2, and the field F_l and profile η as per Figure 3 (respectively, the first and third sub-plot). Interestingly, the optimal profile is indeed "bang-bang" and resembles that studied in [1]. Here however, this profile is an *outcome* of the design, rather than a starting point (as in [6] for example).

In examining the distribution of field power, note that the field tends to intensify in regions of high refractive index. In this case, this region corresponds to the boundary of the fibre (the right hand end, $r = 1$). Hence, the exterior of the fibre tends to support more power than the core region immediately surrounding the fibre axis. This is essential in providing a high field intensity at the fibre / environment boundary which promotes a larger evanescent field supported in the surrounding environment.

C. Case II: Refractive index design with rate constraints

An additional design requirement to the specifications of Case I might be to enforce a refractive index rate constraint (expressed in the normalized radial coordiate r) of the form

$$\left|\frac{dn}{dr}\right| \leq 10\,(n_{\max} - n_{\min})\,, \quad r \in (0,1]. \tag{23}$$

That is, full scale deflections in refractive index can occur over at most 10% of the fibre radius. This rate constraint reflects reasonable estimates for current manufacturing processes [4]. Whilst not shown (due to lack of space), the resulting profile implements this rate constraint at the cost of reduced evanescent field power. For the interested reader, the effect of an identical rate constraint on communications fibre design is presented later in this paper.

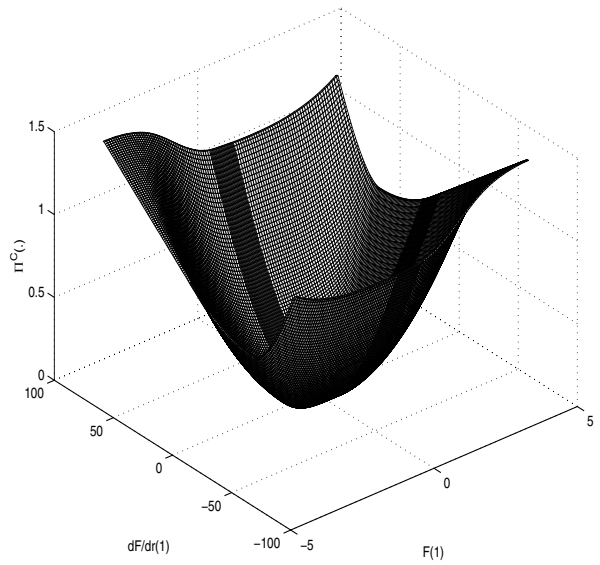

Fig. 2. Sensor fibre case I (without rate constraint), $\Pi^C_{l,\beta}$.

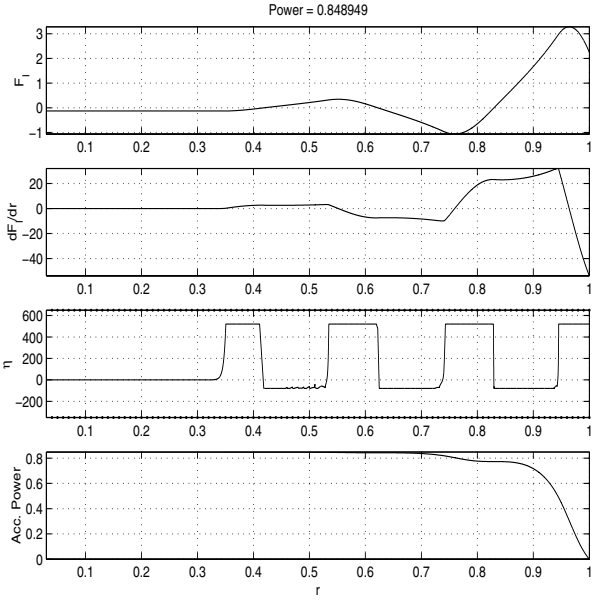

Fig. 3. Sensor fibre case I (without rate constraint), field and profile.

V. Communications fibre design

A. Theory

In designing optical fibre for communications purposes, the objective is to minimize the evanescent field, thereby maximizing the containment of the field within the fibre itself. To this end, the problem formulation is similar to that of the sensor problem, with the refractive index profile (or rate profile) defined by the minimizer of $\overline{\mathcal{P}}(\mathbf{E}_{l,\beta,n})$ in (16). Following similar reasoning as in the sensor case yields an analogous definition to (18) of the maximal power in the fibre, with the infemum replaced by a supremum,

$$\Pi^C_{l,\beta}(x) = \sup_{u\in\mathcal{U}(0,1]} \left\{ \mathcal{P}(0,1;F_{l,\beta,n}) \;\middle|\; \begin{array}{l} \text{(8), (9), (12)} \\ \text{and (13) hold} \\ \text{with } x(1) = x \end{array} \right\} \tag{24}$$

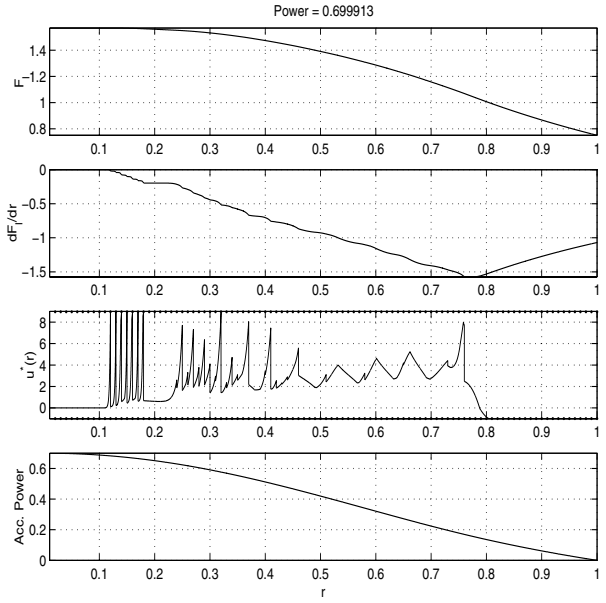

Fig. 4. Communications fibre case I (without rate constraint).

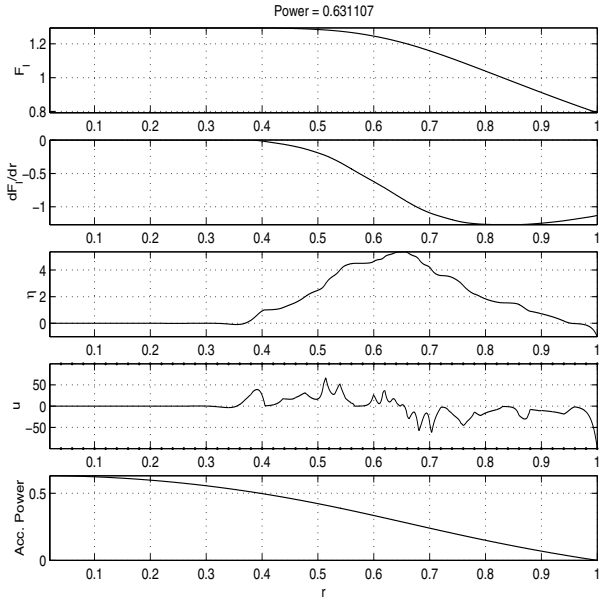

Fig. 5. Communications fibre case II (with rate constraint).

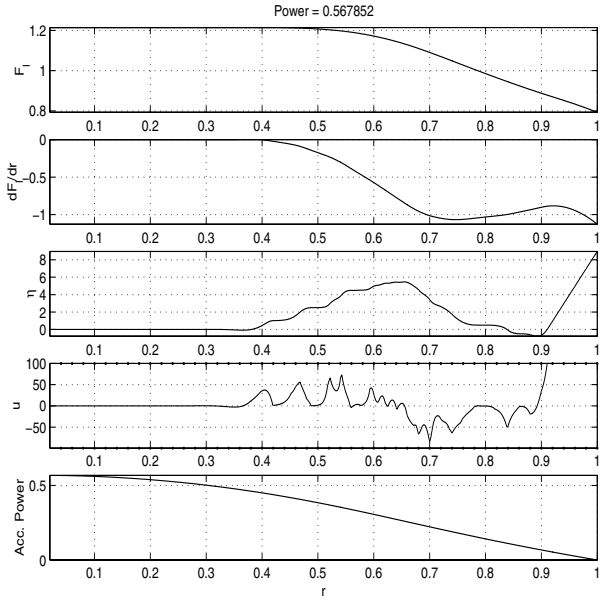

Fig. 6. Communications fibre case III (with rate constraint).

The DPE follows in a similar manner, yielding

$$0 = x_1^2 x_4 - \inf_{u \in \mathbf{U}} \left\{ \nabla_x \Pi_{l,\beta}^C(x) \cdot f(x,u) \right\}, \qquad (25)$$

with boundary conditions identical to (21) with the exception that ∞ is replaced by $-\infty$. Finally, it should be noted that the evanescent field power $\Pi_{l,\beta}^E$ is identical to that of the sensor case, except that the "environment" actually consists of the cladding with index n_{cl} surrounded by an external medium of index n_e. That is, the environment actually exhibits a step index profile, requiring computation of slightly different modified Bessel function solutions to that of the sensor case.

B. Case I: Refractive index design without rate constraints

A communications fibre with the following physical parameters is to be designed:

$$\begin{array}{rclrcl} n_{\min} & = & 1.490 & R & = & 4.50\,\mu m \\ n_{\max} & = & 1.500 & \lambda & = & 1550\,nm \\ n_e & = & n_{\min} & l & = & 0 \\ n_{\text{eff}} & = & 1.491 & \beta & = & 6.044 \times 10^6\, m^{-1} \\ n_{\text{cl}} & = & n_{\min} & \gamma_{l,\beta,n_e} & = & -1.425 \end{array}$$

Without refractive index rate constraints, the obtained refractive index profile η shown in Figure 4 (sub-plot 3) exhibits significant sharp changes and peaks. Of particular interest is the periodic structure, which implies a potentially considerable (and practically undesirable) wavelength dependence of the transmission gain of the fibre. That is, loss along the fibre may be very sensitive to laser wavelength [5].

C. Cases II & III: Refractive index design with rate constraints

Introducing the same refractive index rate constraints (23) as in the sensor case yields a considerably more practical profile, as shown in Figure 5. Naturally, this rate constraint has the effect of reducing the field power confined to the $9\,\mu m$ "core" (i.e. $r \in (0,1]$), but that is to be expected. Finally, it is of interest to note that due to the low n_{eff} selected in this case, a substantial "barrier" refractive index is induced in the region of 0.6 to 0.7 normalized radii. Internal reflection is thus obtained (to some extent) at the outer boundary of this barrier. To further demonstrate this, Figure 6 illustrates the case where the cladding index is high, showing that the barrier feature is retained to discourage a high evanescent field that would otherwise eventuate.

VI. Conclusion

The application of dynamic programming and associated numerical methods was applied to the solution of two optical device design problems. The results provided some interesting physical insight into the effects of refractive index rate constraints on the performance and manufacturability of such devices.

APPENDIX
NUMERICAL METHOD

The DPEs (20) and (25) are both first order nonlinear partial differential equations that rarely admit closed form analytical solutions. Numerical solution methods must be employed in order to compute the power $\Pi^C_{l,\beta}$ inside the fibre in both cases.

Using techniques similar to those in [7], finite differences can be applied to DPEs (20) and (25), yielding a value space iterative method for computing both $\Pi^C_{l,\beta}$ and the corresponding optimal refractive index feedback strategy. Before presenting this iterative method, we first define the following non-uniformly spaced grid in the state space:

$$G_X = \{x \in \mathbf{R}^4 : |x|_\infty \leq K_X\} \cap \mathcal{G}_\infty. \tag{26}$$

Here $K_X < \infty$ is a bound on the state space grid, and $\mathcal{G}_\infty$ is defined recursively as

$$\begin{aligned} \mathcal{G}_0 &= \{0\},\ 0 \in \mathbf{R}^4, \\ \mathcal{G}_{j+1} &= \mathcal{G}_j \cup_{\substack{i=1\ldots n \\ x \in \mathcal{G}_j}} \{x + \delta_i^+(x)e_i, x - \delta_i^-(x)e_i\}, \end{aligned}$$

where e_i is the i^{th} orthonormal basis vector in $\mathbf{R}^4$, $\delta_i^\pm(x)$ are the grid spacings in directions $\pm e_i$ at $x \in \mathbf{R}^4$. Similarly, a uniform grid G_U is used for approximating the refractive index rate input, with spacing δ_U and bound K_U:

$$G_U = \{u \in \mathbf{R} : |u| \leq K_U\} \cap (\mathbf{R})^{\delta_U}.$$

Here $(\mathbf{R})^{\delta_U}$ denotes the unbounded lattice of points in $\mathbf{R}$ with spacing δ_U. A backward difference approximation for the gradient of $\Pi^C_{l,\beta}(x)$ in direction e^i can then be defined on the simplex $N(x)$ in G_X as shown in Figure 7:

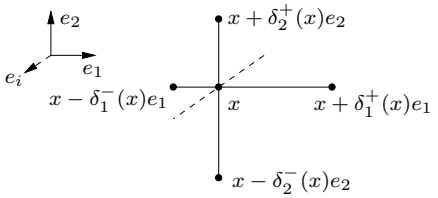

Fig. 7. Simplex $N(x)$ centered on $x \in \mathbf{R}^2$ in $\mathbf{R}^2$.

$$\begin{aligned} &\tfrac{\partial \Pi^C_{l,\beta}}{\partial x_i} \cdot f_i(x,u) \\ &\approx \begin{cases} \frac{\Pi^C_{l,\beta}(x) - \Pi^C_{l,\beta}(x - \delta_i^-(x)e_i)}{\delta_i^-(x)} & f_i(x,u) > 0, \\ 0 & f_i(x,u) = 0, \\ \frac{\Pi^C_{l,\beta}(x + \delta_i^+(x)e_i) - \Pi^C_{l,\beta}(x)}{\delta_i^+(x)} & f_i(x,u) < 0, \end{cases} \\ &= \left(\frac{\Pi^C_{l,\beta}(x) - \Pi^C_{l,\beta}(x - \delta_i^-(x)e_i)}{\delta_i^-(x)}\right) f_i^+(x,u) \\ &\quad + \left(\frac{\Pi^C_{l,\beta}(x) - \Pi^C_{l,\beta}(x + \delta_i^+(x)e_i)}{\delta_i^+(x)}\right) f_i^-(x,u) \\ &= \left(\frac{f_i^+(x,u)}{\delta_i^-(x)} + \frac{f_i^-(x,u)}{\delta_i^+(x)}\right) \Pi^C_{l,\beta}(x) \\ &\quad - \left(\frac{f_i^-(x,u)}{\delta_i^+(x)}\right) \Pi^C_{l,\beta}(x + \delta_i^+(x)e_i) \\ &\quad - \left(\frac{f_i^+(x,u)}{\delta_i^-(x)}\right) \Pi^C_{l,\beta}(x - \delta_i^-(x)e_i) \end{aligned}$$

where $f(x,u) = [f_1(x,u) \ldots f_4(x,u)]^T$ is defined as per (9), and $f_i^\pm = \begin{cases} \pm f_i & f_i \gtrless 0 \\ 0 & \text{otherwise} \end{cases}$. The directional derivative thus approximated via this backward difference as

$$\begin{aligned} &\nabla_x \Pi^C_{l,\beta} \cdot f(x,u) \\ &= \textstyle\sum_{i=1}^4 \frac{\partial \Pi^C_{l,\beta}}{\partial x} \cdot f_i(x,u) \\ &\approx \Pi^C_{l,\beta}(x) - \textstyle\sum_{i=1}^4 \left(\frac{f_i^-(x,u)}{\delta_i^+(x)}\right) \Pi^C_{l,\beta}(x + \delta_i^+(x)e_i) \\ &\qquad - \textstyle\sum_{i=1}^4 \left(\frac{f_i^+(x,u)}{\delta_i^-(x)}\right) \Pi^C_{l,\beta}(x - \delta_i^-(x)e_i) \\ &- \left(1 - \textstyle\sum_{i=1}^4 \left[\frac{f_i^+(x,u)}{\delta_i^-(x)} + \frac{f_i^-(x,u)}{\delta_i^+(x)}\right]\right) \Pi^C_{l,\beta}(x) \\ &= \Pi^C_{l,\beta}(x) - \textstyle\sum_{z \in N(x)} p(x,z|u) \Pi^C_{l,\beta}(z), \end{aligned}$$

where $p(x,z|u)$ are defined in the obvious way, and may be interpreted as the transition probabilities of a locally consistent Markov chain defined on $N(x)$ in the context of the approximation methods presented in [7]. Clearly $\sum_{z \in N(x)} p(x,z|u) = 1$ for all $x \in G_X$ and all $u \in G_U$. Substitution of this and the discrete approximation $\mathbf{U} \approx G_U$ in (20) (for example) yields

$$\Pi^C_{l,\beta}(x) \approx x_1^2 x_4 + \min_{u \in G_U} \textstyle\sum_{z \in N(x)} p(x,z|u) \Pi^C_{l,\beta}(z),$$

for all $x \in G_X$. Replacing respective instances of $\Pi^C_{l,\beta}$ by $(k+1)^{th}$ and k^{th} approximations yields a contractive value space iteration [7]

$$\left(\Pi^C_{l,\beta}\right)_{k+1}(x) = x_1^2 x_4 + \min_{u \in G_U} \sum_{z \in N(x)} p(x,z|u) \left(\Pi^C_{l,\beta}\right)_k(z), \tag{27}$$

with $\left(\Pi^C_{l,\beta}\right)_0$ satisfying the initialization (21). This defines the numerical scheme used in the sensor design problem. (The communications design scheme uses the analogous iteration and initialization as per (25) and associated discussion.)

REFERENCES

[1] A. Argyros, I.M. Blassett, M.A. Eijkelenborg, M. Large, J. Zagari, N.A. Nicorovici, R.C. McPhedran, and C.M. de Sterke. Ring structures in microstructured polymer optical fibres. *Optics Express*, 9(13):813–820, 2001.

[2] P.M. Dower, P.M. Farrell, and B.G. Gibson. An optimal control problem arising in the design of optical fibre sensors. *To appear, Proc. 43rd IEEE Conference on Decision and Control (Bahamas)*, 2004.

[3] P.M. Dower, P.M. Farrell, and B.G. Gibson. A numerical optimal control approach to the design of an optical fibre-based evanescent field sensor. *To appear, Proc. IFAC World Congress (Prague)*, 2005.

[4] N.M. Dragomir, P.M. Farrell, G.W. Baxter, and A.W. Roberts. Estimation of the refractive index profile of an optical fibre using dic images. *Proc. 25th ACOFT (Canberra)*, pages 126–128, 2000.

[5] N.M. Dragomir, P.M. Farrell, G.W. Baxter, A.J. Stevenson, G. Monnom, F. Brechet, and A. Roberts. Investigating refractive index of photonic band gap fibres using dic microscopy. *Proc. OECC/IOOC Conference (Sydney)*, pages 156–157, 2001.

[6] B.C. Gibson, J.D. Love, L.W. Cahill, P.M. Dower, and D.M. Elton. Evanescent field analysis of air-silica microstructure waveguides. *Proc. 14th Annual Meeting of the IEEE Lasers & Electro-Optics Society, LEOS (San Diego, USA)*, 2:709–710, 2001.

[7] H.J. Kushner and P.G. Dupuis. *Numerical methods for stochastic control problems in continuous time*. Springer-Verlag, 1992.

[8] A. Snyder and J.D. Love. *Optical waveguide theory*. Chapman and Hall, London, 1983.